An Overset Unstructured Mesh Discontinuous Galerkin Approach for Aerodynamic Problems

Cristian R. Nastase * Dimitri J. Mavriplis † Jay Sitaraman ‡

Department of Mechanical Engineering, University of Wyoming, Laramie, WY 82071

We present a novel approach for the simulation of aerodynamic configurations where vortical and wake effects are important. The approach makes use of a well established Reynolds-averaged Navier-Stokes unstructured mesh solver in the region near the body geometry, in order to efficiently handle the associated geometric complexity in these regions. In the off-body regions, a high-order (up to 6th order) accurate Discontinuous Galerkin discretization is used to accurately capture wake and vortical effects. The near body and off-body solvers operate on separate overlapping meshes and a separate software module is invoked to compute and manage the time-dependent interpolations between the two grid systems. The approach is demonstrated on the canonical problem of an isentropic convecting vortex and for the steady-state flow over a lifting wing with resolved wing tip vortex.

I. Introduction

Over the past decade high-fidelity simulations based on solutions of the Reynolds-Averaged Navier Stokes (RANS) equations have been progressively applied to more complex configurations, including rotorcraft configurations with relative component motion .[1–6] Many of these approaches use body-fitted structured or unstructured meshes within an overset mesh framework. Specifically, the OVERFLOW[7] code utilizes a dual-mesh approach with structured body-fitted meshes applied near the body and with Cartesian meshes in wake regions. Moreover, the benefits of high-order schemes have been shown to be important for performance predictions and for accurate vortex and wake capturing by Hariharan,[8] Sankar,[9] Yeshala,[10] and Duque et. al.[11] Despite these advances, routine use of these tools by design engineers remains limited.

Recently, an overset approach which combines the advantages of unstructured mesh technology for discretizing complex geometries with the efficiency and accuracy of high-order finite-difference schemes on adaptive Cartesian meshes for capturing wakes and vortices has been used to compute highly accurate solutions of rotor flows with highly resolved wake features.[12] In this approach, the unstructured mesh solver is used in the near body region, where geometrical complexity dominates, and the Cartesian mesh is used in the off-body region where wake and vortical effects must be resolved.

In this paper, we investigate the effectiveness of an alternate strategy where the off-body Cartesian finite difference solver is replaced with an off-body high-order accurate discontinuous Galerkin solver. Discontinuous Galerkin (DG) methods have become the subject of intensive research over the last decade due to their superior asymptotic accuracy properties and their ability to operate on arbitrary mesh types. However, substantial issues remain to make DG methods suitable for production use on complex industrial cases. These include the requirement of generating curved mesh elements in near boundary regions, as well as numerous robustness issues associated with capturing non-smooth flow features such as shocks, and non-smooth turbulence modeling effects.[13,14] The use of a DG method as an off-body solver for aerodynamic simulations bypasses many of these issues while capitalizing on the most effective advantages of DG discretizations, namely the ability to deliver high accuracy for smooth flow phenomena with relatively low grid resolution. However, DG solvers are known to be relatively expensive, particularly when compared with simpler finite-difference Cartesian methods, which can also attain higher-order accuracy. Nevertheless, DG

*Research Scientist, AIAA member; email: nastase@uwyo.edu

†Professor, AIAA Associate Fellow; email: mavriplis@uwyo.edu

‡Assistant Professor, AIAA Member; email: jsitaraman@uwyo.edu

discretizations offer several advantages which are worthy of investigation and which may lead to an overall more flexible and efficient approach. Firstly, high-order DG discretizations operate with compact stencils and sub-cell resolution (i.e. with increasing numbers of degrees of freedom per cell as the order is raised). The use of compact stencils means that complications due to halo or ghost cells arising in adaptive meshing and overset mesh interpolation are minimized, and boundary conditions may be implemented in a straightforward manner. Additionally, the level of mesh refinement required to achieve a prescribed accuracy will be much lower with a DG method than with a finite-difference approach (although the total number of degrees of freedom can be expected to be similar). This in turn simplifies many of the mesh-based operations including adaptive refinement and load balancing, many of which are becoming the bottlenecks in large-scale parallel simulations. DG discretizations also enable the use of p-refinement (or order refinement) instead of h-refinement(or mesh refinement), particularly for smooth flow features as one may expect in off-body regions. DG discretizations also are known to scale very well on massively parallel computer architectures, even for relatively coarse meshes. Finally, DG methods may be applied to Cartesian hexahedral element meshes, as well as unstructured meshes with any combination of element types (tetrahedral, hexahedral, prismatic etc.) providing added flexibility compared to finite-difference Cartesian methods. Ultimately, the use of a DG approach for off-body regions may be viewed as a preliminary step in the development of an overset framework which has the option of using DG discretizations in both near-body and off-body regions.

In the following sections, we first describe briefly the second-order accurate finite volume solver used in the near-body regions, followed by a description of the DG solver used in the off-body region, and the coupling between these two codes. In the results section, we validate the overset finite-volume / DG approach by simulating the canonical problem of a isentropic convecting vortex and by computing the flow over a lifting wing with a resolved wing tip vortex.

II. Solver Modules

The multi-solver approach employs legacy flow CFD solvers for the near-body region and the high-order DG solver for off-body regions. A Python integration framework is used to couple the near-body and off-body solvers. The framework makes use of standardized interfaces such that additional solvers that conform to the interface may be substituted in the place of existing solvers. A description of the solvers and integration framework is given below.

II.A. Near-Body Finite-Volume Flow Solver

The structured mesh Reynolds averaged Navier-Stokes solver TURNS[15] is used as the near body solver. TURNS uses a finite volume node-centered upwind numerical algorithm to discretize the governing equations. In this algorithm, the evaluation of the inviscid fluxes is based on an upwind-biased flux-difference scheme originally developed by Roe.[16] The LU-SGS scheme developed by Jameson and Yoon[17] is used for the implicit operator. For time-accurate computations a second-order backward difference in time is used, along with Newton-type sub-iterations to remove factorization errors and restore formal second order accuracy. The TURNS code supports dynamically deforming meshes and iblanking for overset mesh simulations, and has been utilized for a variety of fixed-wing and rotary-wing problems and is validated for related aerodynamic flows.[18]

The NSU3D unstructured mesh finite-volume solver is also available for use as a near-body flow solver.[19,20] Both TURNS and NSU3D support the Python interfaces used to integrate the near-body and off-body solvers and can be used interchangeably.[20] However, in the current work, only the TURNS code has been used as a near-body solver.

II.B. Discontinuous Galerkin Off-Body Solver

The off-body discontinuous Galerkin code is based on the DG discretization and solver described in references.[14,21–23] The discretization approach uses element-based basis functions that are discontinuous at the element interfaces. In particular, a set of hierarchical basis functions based on variable weight Jacobi polynomials defined within a standard isoparametric element are used. For the convective terms, the inter-cell discontinuity is resolved using a numerical flux, which provides inter-cell communication and boundary condition enforcement on the convective flux. The inter-cell numerical flux is obtained as a solution of a local one-dimensional Riemann problem and depends on the internal interface states at the two adjacent

elements. An approximate Riemann solver is used to compute the flux at inter-element boundaries. Current implementations include the flux difference splitting schemes of Rusanov, Roe, HLL and HLLC.

Viscous terms for the Navier-Stokes equations are implemented using the symmetric interior penalty (SIP) method, although the off-body simulations performed in this work only consider the solution of the Euler equations, under the assumption that the dominant viscous effects occur near the body and are modeled by the near-body solver.

The current three-dimensional implementation includes discretizations up to p=5 (6th-order accurate) for tetrahedral, hexahedral, prismatic, and pyramidal elements, and arbitrary mixtures of these elements within an unstructured mesh can be handled. Elements are required to be conforming (i.e. no hanging nodes), although the implementation of non-conforming elements is planned in the near future. Additionally, elements may have variable order, under the constraint that the order of two neighboring elements can differ by at most $|p_{left} - p_{right}| = 1$.

Temporal integration schemes include first and second-order backwards difference (BDF1 and BDF2) methods, a Crank-Nicolson implicit time-stepping scheme (CN2) as well as first, second and third-order accurate explicit Runge-Kutta schemes. The non-linear system arising at each implicit time step (or for a steady-state calculation) is solved using a h-p multigrid approach driven by an element Jacobi smoother.[21,24] In this approach, only the Jacobian matrix blocks corresponding to the coupling between all degrees of freedom within a mesh element are considered, and these dense blocks are inverted using an LU factorization procedure. This procedure is repeated on each level of the multigrid sequence, where the order (and thus block size) is reduced on each successively coarser level until a p=0 (1st order accurate) discretization is reached, which is then solved using a traditional agglomeration (h-) multigrid approach.

For operation within an overset environment, a similar "iblanking" capability to that described for the near body solvers has been implemented. The "iblanks" specify at which nodes the solution variables are to be updated (iblank = 1) and which nodes are not updated, i.e., fringes and holes (iblank = 0). The fringes correspond to the overset regions that receive information from the near-body grid, while holes correspond to locations where the off-body grid is inactive and the near-body grid is dominant.

II.C. Overset grid assembly

Overset grid assembly involves developing donor-recipient relationships and interpolation strategies between mutually overlapping meshes. The overall solution procedure for the overset meshes is as follows. At each iteration step, the solutions of the fluid equations in each mesh are obtained independently with the solution in each fringe region being specified by interpolation from the overlapping "donor" mesh as a Dirichlet boundary condition. At the end of the iteration, the fringe data are exchanged between the solvers so that the evolution of the global solution is consistently represented by the overset methodology. The approach used in this paper uses an explicit hole-cutting method to identify potential recipients. All the outer boundary grid nodes of the near-body mesh (i.e. the mesh that conforms to the solid boundary) are identified as potential recipients and donor cells are sought for these nodes. For the DG off-body solver, the identification of potential recipients is a two step process. First, a ray tracing based hole-cutting is performed with a grid surface (which is a specified distance from the outer boundary) as the cutter. All the cells inside the cutter surface are tagged as potential donor cells, except those that are found inside the solid wall boundary. In the second step, based on the polynomial order of the DG-scheme, additional points (required by the DG projection scheme) are generated in each cell, which forms the final list of recipient grid nodes. Donor search for all the potential recipients are performed in a fully parallel way. We utilize the CHIMPS+ software [25,26] to perform all the hole-cutting, donor search and data interpolations. CHIMPS+ utilizes an Alternating Digital Tree (ADT) based meta-data structure to accelerate the searches.

Trilinear interpolation is used to transfer data at the fringe points between near and off-body meshes. The off-body mesh resolution is generally coarser than the near body resolution, and values from the near body to the off-body are interpolated to the set of additional points created within each mesh cell trilinearly from their enclosing near body mesh cells. Because the DG discretization operates in modal space, these nodal values within each DG cell are then used to reconstruct the modal coefficients of the interpolating polynomial within the cell. A minimum number of $(p+1)^3$ interpolating points are required to generate the unique interpolating cell polynomial of order p. Thus, for p=1, 8 sub-cell vertices are used, whereas for p=2,3 and 4, 27, 64 and 125 points are required, respectively. When interpolating from the off-body to the near-body grid, the corresponding transpose operations are used: solution values are projected from the cell polynomial representation to the sub-cell interpolating points, and these are interpolated trilinearly to the

near-body cells.

II.D. Time Integration Controller

The multi-code infrastructure consists of two parts: (1) a general high-level Python script or execution interface that controls the execution of different modules, and (2) a set of module-specific interfaces, that are callable by the Python script. The Python infrastructure is designed to maximize the throughput and minimize memory overheads. Each code allocates its own memory and data pointers are used to access data, rather than packing and unpacking exchange buffers. The object-oriented interfaces are defined to standardize the data exchange between different participant solvers, which facilitates the replacement and/or addition of new solvers. The individual near-body and off-body solution processes are controlled by the Python main program, which orchestrates the overall iterative or time-integration procedure. For steady-state cases, the main program controls the outer iterative loop. At each iteration level, the near- and off-body solvers execute a single iteration and at the end of the iteration, the solvers exchange fringe data through the domain connectivity module. The iterative process continues until some overall convergence measures are attained, at which point, both solvers output their respective data and the program execution terminates. We note that the independent solvers have their own iterative solution procedures: block- and line-implicit solution for NSU3D, LU-SGS for TURNS. The off-body DG solver includes a steady-state element Jacobi solver, first and second-order backwards difference (BDF1 and BDF2) methods, Crank-Nicolson implicit time-stepping scheme (CN2) as well as first, second and third-order accurate explicit Runge-Kutta schemes. The integration controller does not specify the pseudo-time selection in the candidate solvers and only keeps track of the outer iteration counter and the data exchange at the end of each iteration. In principle, each of the solvers can also perform a specified number of inner sub-iterations if desired (say, for load balancing purposes), but this feature is not presently used.

III. Results

The results section is organized as follows: Isentropic vortex convection in inviscid flow is investigated first to assess the accuracy of the proposed multi-code paradigm. Finally, results of high Reynolds number steady viscous turbulent flow over a NACA0015 wing are presented along with comparison to wind-tunnel test data.

III.A. Isentropic Vortex

One of the objectives of this work is to systematically investigate the accuracy of the overset mesh multi-code framework using the canonical problem of an isentropic convecting vortex with a known exact solution. The problem consists of initializing the exact solution of the vortex and integrating it in time as it convects downstream in a uniform flow environment. Comparison of the computational solution with the exact solution provides a precise measure of the dissipation and dispersion errors in the solution procedure. In particular, the test case allow us to assess the effects of combining disparate numerical schemes and the performance of the overset data exchange strategy. Moreover, it provides an evaluation of the benefits of using higher-order discretizations in the off-body solution.

The 3D geometry consists of a straight duct with the free-stream flow in the axial direction and inviscid wall boundary conditions enforced on the side boundaries. The off-body DG mesh is a purely hexahedral mesh with $NX = 41, NY = 14, NZ = 8$ cells in the streamwise, vertical, and cross-flow directions, respectively, for a total of 4592 cells. The near-body mesh is chosen to be finer than the off-body mesh to account for the second-order accuracy of the near-body solver compared with the variable-order accuracy of the off-body solver. The near-body mesh is a Cartesian mesh of size $NX = 45, NY = 45, NZ = 33$ for a total of 66,825 cells, and this mesh is embedded in a subregion corresponding to $NX = 7, NY = 7, NZ = 8$ cells of the DG off-body mesh, as seen in Figures 1 and 2. The vortex is initialized within the embedded near-body mesh and then convects out of the near body mesh into the off-body DG mesh.

All computations are performed at a Mach number of 0.5 and a time step $dt = 0.2$. The mean flow density, ρ_∞, velocity, u_∞ and v_∞, pressure, p_∞ and temperature T_∞ are taken as free stream values, which are set as $(\rho_\infty, u_\infty, v_\infty, p_\infty, T_\infty) = (1, 0.5, 0, 1/\gamma, 1)$ in this test case. The flow is perturbed by an isentropic vortex $(\delta u, \delta v, \delta T)$ centered at (x_0, y_0) with the form:

$$\delta u = -\frac{\alpha}{2\pi}(y - y_0)e^{\phi(1-r^2)} \tag{1}$$

$$\delta v = \frac{\alpha}{2\pi}(x - x_0)e^{\phi(1-r^2)} \tag{2}$$

$$\delta T = -\frac{\alpha^2(\gamma - 1)}{16\phi\gamma\pi^2}e^{2\phi(1-r^2)} \tag{3}$$

where, ϕ and α are parameters which determine the strength of the vortex, $r = \sqrt{(x - x_0)^2 + (y - y_0)^2}$ is the distance to the vortex center, and $\gamma = 1.4$ is the ratio of specific heats. In this study, we set ϕ as unity and α as 4.0. Given the perturbation functions shown in Eq. 1, 2 and 3, we can determine the other resulting conservative variables, assuming isentropic flow throughout the domain:

$$\rho = T^{1/(\gamma-1)} = (T_\infty + \delta T)^{1/(\gamma-1)} = \left[1 - \frac{\alpha^2(\gamma - 1)}{16\phi\gamma\pi^2}e^{2\phi(1-r^2)}\right]^{1/(\gamma-1)} \tag{4}$$

$$u = u_\infty + \delta u = 0.5 - \frac{\alpha}{2\pi}(y - y_0)e^{\phi(1-r^2)} \tag{5}$$

$$v = v_\infty + \delta v = 0 + \frac{\alpha}{2\pi}(x - x_0)e^{\phi(1-r^2)} \tag{6}$$

The initial vortex ($t = 0$) is placed at $(x_0, y_0) = (7.5, 3.5)$ as depicted in Figure 1(a) and is convected to $x = 17.5$ which corresponds to a displacement in $x-$direction of $dx = 20$.

For comparison purposes, the vortex problem is also computed using the stand-alone DG code with tetrahedral and hexahedral meshes. Figures 3 (a) and (b) illustrates the vortex solution obtained using the DG solver alone on a tetrahedral mesh of order $p = 4$ and on a hexahedral mesh of order $p = 3$, respectively. Additionally, a prescribed variable p-order mesh is constructed where a band of cells in the center of the mesh (containing the path of the vortex) are set to p=4 (5th-order) accuracy, while the remaining cells are set to lower accuracy orders. Figure 3(c) shows the mesh cell prescribed accuracy order distribution for the variable order case.

Figure 1 and Figure 2 show density contour plots in the mid $z-$direction plane at various dowstream locations using the overset mesh approach with $p = 1$ and $p = 3$ DG discretizations, respectively. Figure 4 shows the density profiles in the y-direction at the $x = 17.5$ plane downstream location for the exact, baseline and overset solutions. The exact solution is obtained by projecting the analytic vortex definition onto the corresponding $p-$order basis set at the appropriate downstream location. The DG baseline denotes the solution obtained via the DG solver alone, either on the hexahedral mesh at uniform prescribed order (c.f. Figure 3(b)) or on the variable order mesh (c.f. Figure 3(c)). For the $p = 1$ solution, the vortex profile is slightly diffused compared to the exact solution, both for the overset-mesh and stand-alone DG solutions, whereas for the higher order DG solutions, good agreement is observed between the overset mesh, stand-alone DG and exact solutions. These results demonstrate that the errors introduced by the interpolation process as the vortex transitions from the near-body to the off-body mesh are small enough to avoid corrupting the accuracy of the underlying DG discretization. Additionally, the variable order results shown in Figure 4(d) illustrate the potential for achieving computational savings through prescribed or adaptive p-order distributions, which can be incorporated relatively easily within the DG framework.

III.B. Flow over a NACA0015 wing

The multi-code approach is next used to study the flow-field over a NACA 0015 rectangular wing. The primary objective of this computation is to verify and test the integrity of the multi-code simulation capability for a high-Reynolds number turbulent external flow problem. The experimental data used for validation are those measured by McCalister et.al.[27] The wing geometry is a rectangular planform with a square-tip and has an aspect ratio of 3.3. The test point for which validation results are presented is at the following operating condition : $Mach = 0.1235$, $Re = 1.5e^6$, $\alpha = 12^o$. For this case, computations are performed by using both the structured curvilinear (TURNS) near-body solver, and the DG solver for the off-body solver.

Figure 5(a) and Figure 5(b) shows the contours of Y-momentum (ρV) and Z-momentum(ρW), respectively. The contours of Z-momentum qualitatively represents the downwash distribution and hence provides

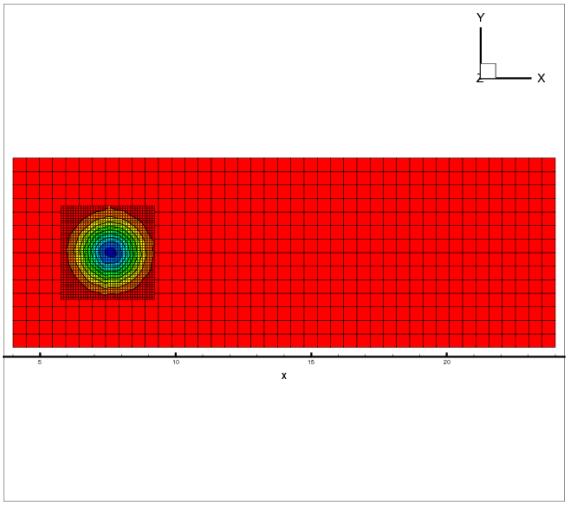

(a) x=7.5

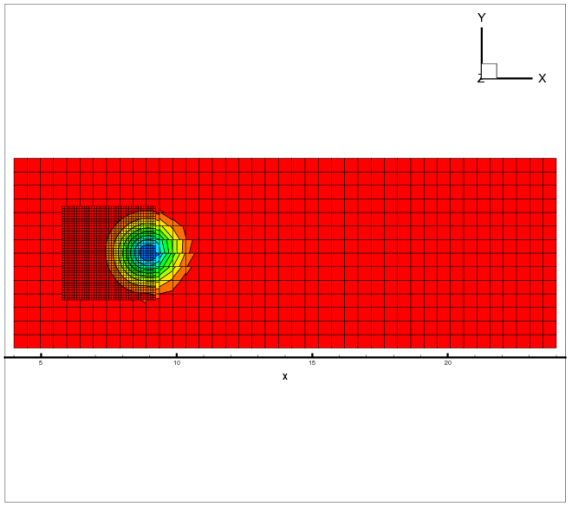

(b) x=9

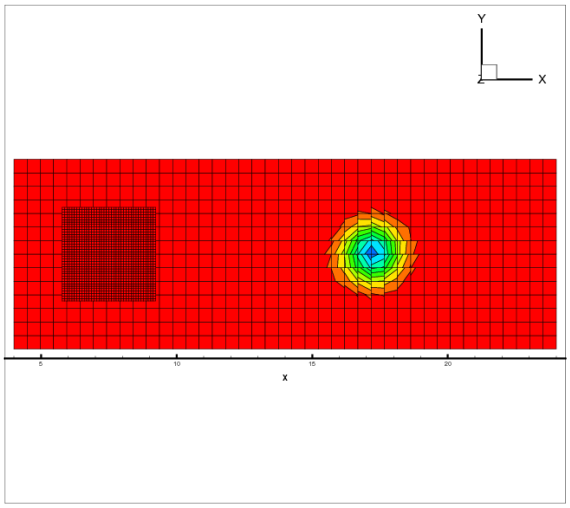

(c) x=13

Figure 1. Overset solution of vortex convection using a $p = 1$ spatial discretization with a BDF2 temporal discretization at various streamwise locations.

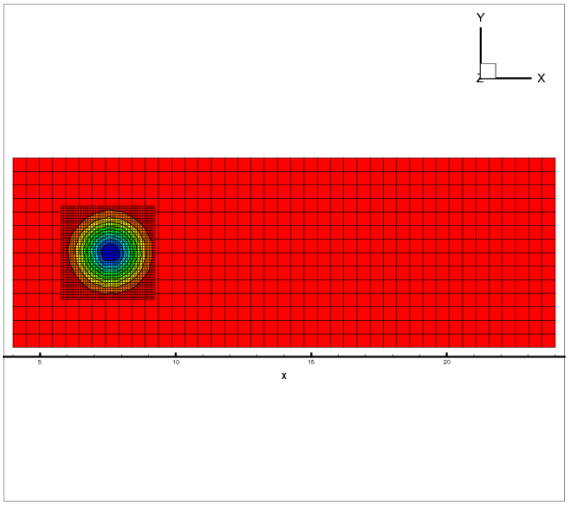

(a) x=3

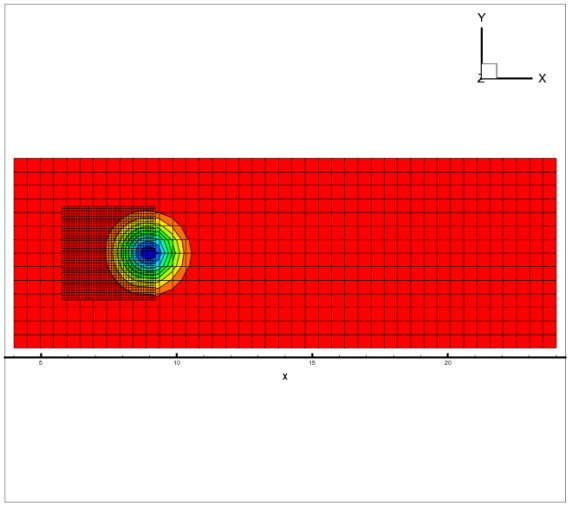

(b) x=9

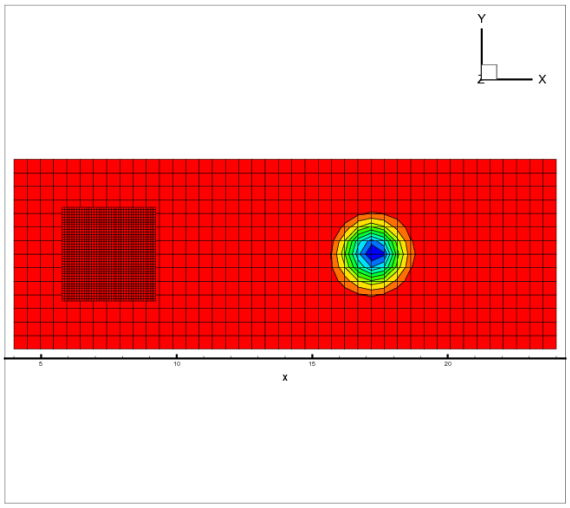

(c) x=13

Figure 2. Overset solution of vortex convection using a $p = 3$ spatial discretization with a BDF2 temporal discretization at various streamwise locations.

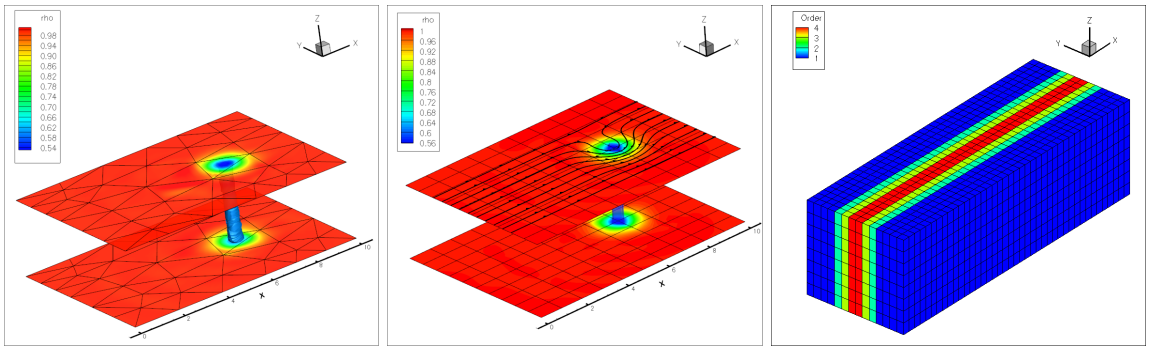

(a) (b) (c)

Figure 3. DG solution of vortex convection using (a) tetrahedral mesh and p=4 discretization with a BDF2 temporal discretization and (b) hexhedral mesh p=3 spatial accuracy and a CN2 temporal discretization.(c) Variable order distribution used for vortex convection problem.

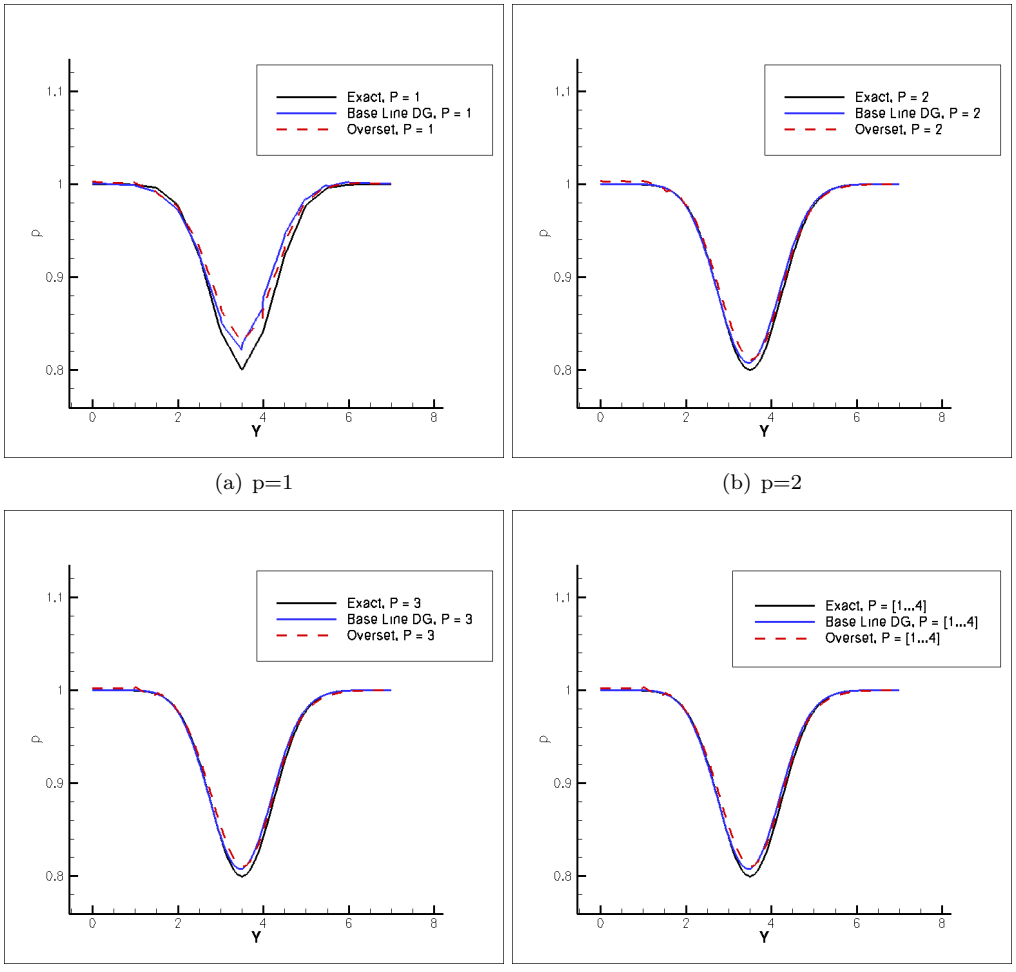

(a) p=1 (b) p=2

(c) p=3 (d) Variable order

Figure 4. Density profiles in y-plane at $x = 17.5$ downstream location for exact, baseline and overset solutions.

insight into the physics of the flow field. As expected, the flow field is dominated by the presence of a vortex sheet which rolls up into a coherent tip vortex close to the wing. This tip vortex remains coherent within the computational domain as depicted Figure 5(c).

Figure 6 displays the load variation along the full wing span. Results obtain from $p = 1$ and $p = 2$ computation are plotted against experimental data. Fair agreement can be noted between the measurement and prediction.

The downstream development of the trailing vortex is qualitatively represented by the swirl velocities. Figure 7 shows the comparison of swirl velocities predicted at the tip-vortex locations for the $p = 1$ DG discretization with measured experimental data at various x/c downstream locations. The peak magnitudes of the trailing vortex are seen to be underpredicted for this simulation. The use of a finer near body mesh and a higher-order DG discretization are required to improve the prediction of these peak velocities.

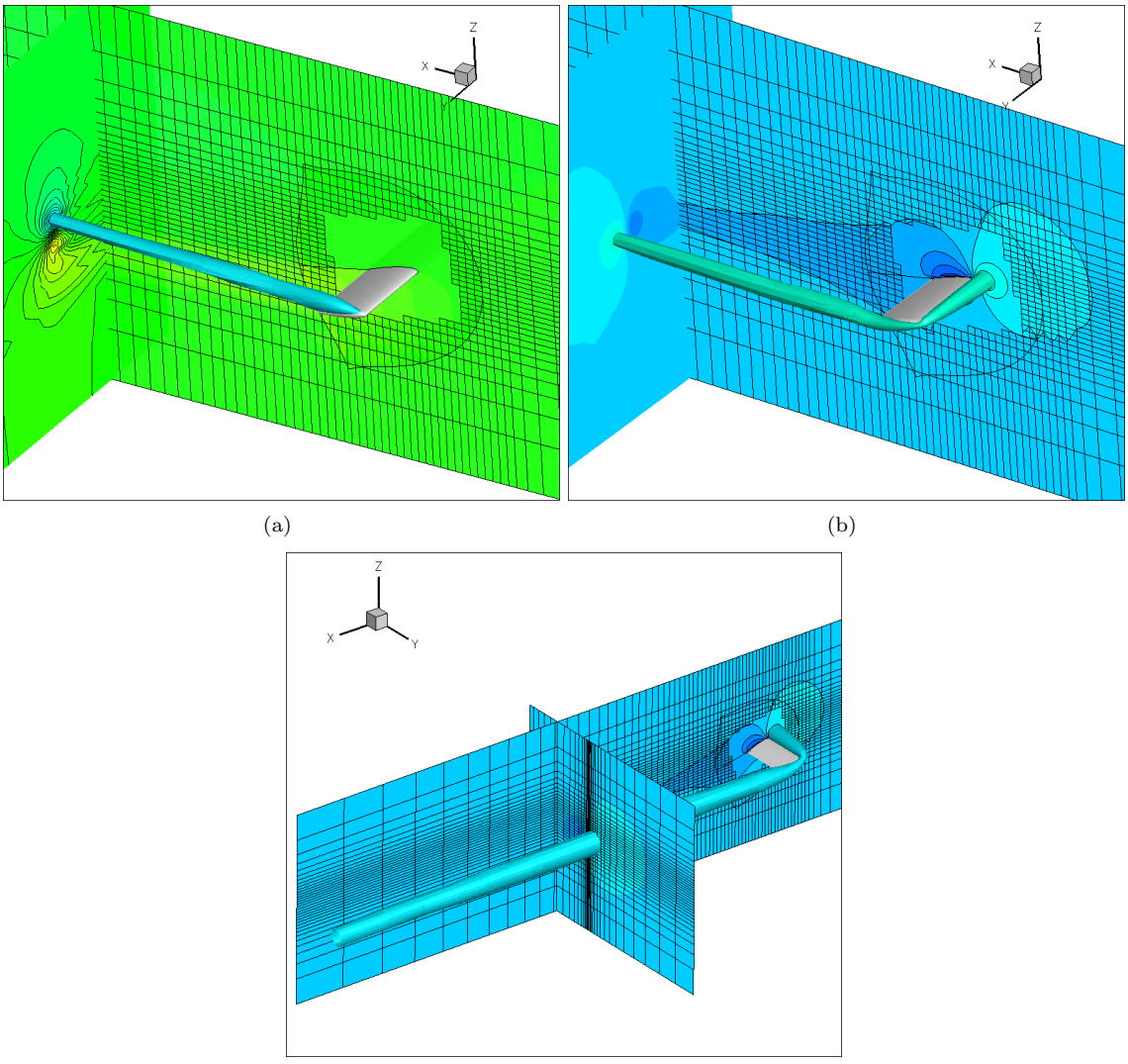

Figure 5. Illustration of composite overlapping meshes and captured wing tip vortex for flow over wing for p=1 DG discretization.

IV. Future Work

In this work, we have demonstrated and validated an overset mesh approach using a high-order accurate discontinuous Galerkin discretization in off-body regions in conjunction with a more traditional second-order accurate finite-volume approach in near body regions. The approach capitalizes on the advantages of DG

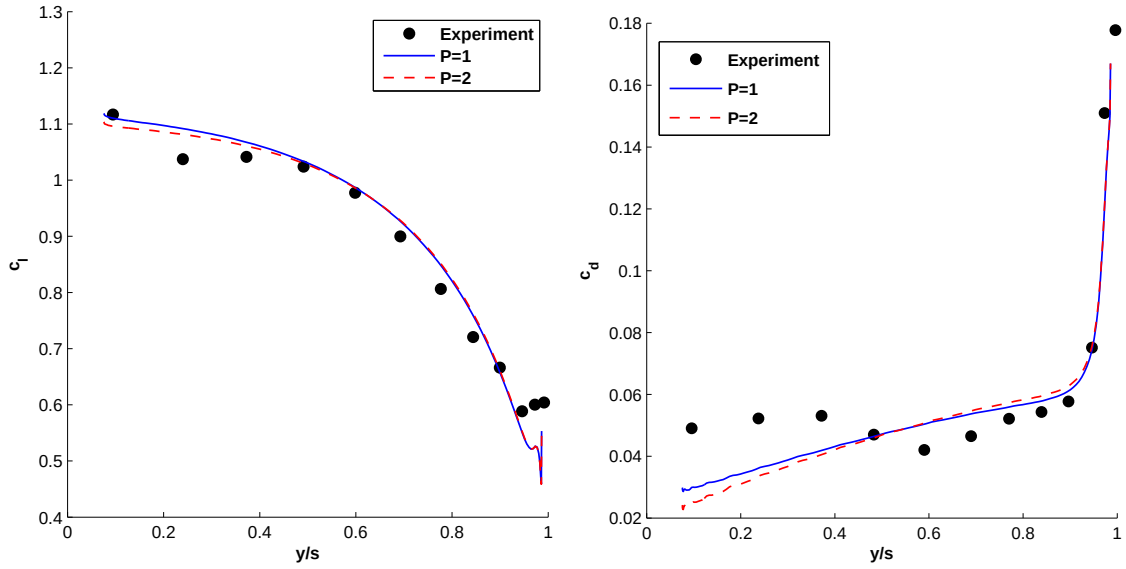

(a) c_l (b) c_d

Figure 6. Load variation along full wing span for solution using p=1 and p=2 DG discretizations.

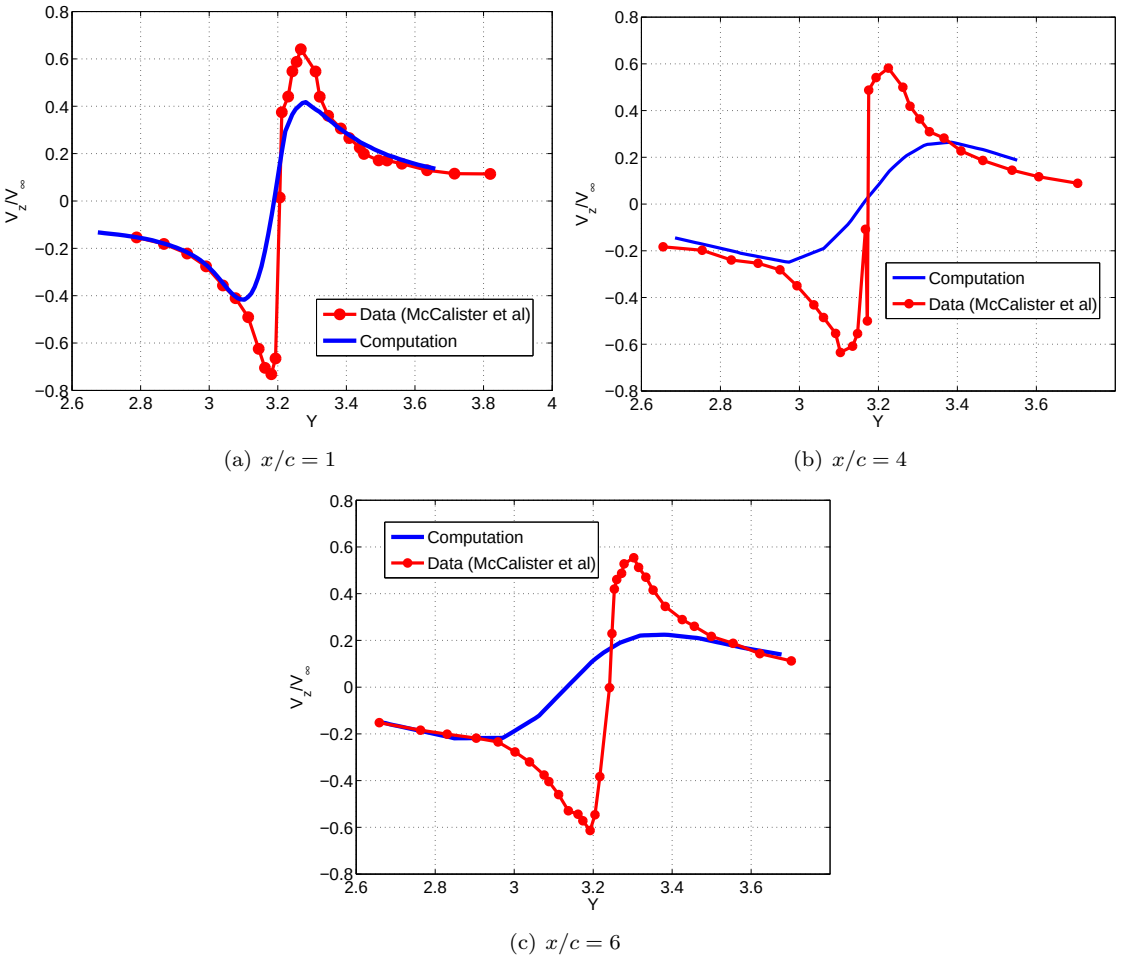

(a) $x/c = 1$ (b) $x/c = 4$

(c) $x/c = 6$

Figure 7. Comparison of predicted swirl velocities with experimental data at various downstream locations for solution using p=1 DG discretization.

discretizations, namely high accuracy, compact stencils, adaptive order capabilities, low mesh resolution and associated infrastructure costs, and good overall scalability. At the same time, this approach sidesteps many of the obstacles that inhibit industrial use of DG methods such as the need to generate curved element meshes and robustness issues for non-smooth solutions. By conforming to a standard set of Python-based interfaces, the DG solver may be substituted within the multi-code framework using alternate solvers with minimal effort. The grid assembly, hole-cutting and interpolation setup operates in parallel and supports dynamic mesh motion for time-dependent simulations. In future work, the high-order DG solver will be used as the off-body solver for the simulation of time-dependent problems with dynamic mesh motion, for example involving rotating configurations such as a helicopter or wind turbine rotor. Additionally, alternate near-body solvers including an unstructured mesh finite-volume solver will be used in conjunction with the off-body DG solver. In the longer term, an overset DG approach involving both near-body and off-body DG discretizations will be pursued.

V. Acknowledgements

This work was supported by AFOSR under contract number FA9950-10-C-0051.

References

[1]Wake, B. and Baeder, J., "Evaluation of a Navier-Stokes Analysis Method for Hover Performance Prediction," *Journal of the American Helicopter Society*, Vol. 41, No. 7, 1996.

[2]Ahmad, J. and Strawn, R., "Hovering Rotor and Wake Calculations with an Overset-Grid Navier-Stokes Solver," *Proceedings of the American Helicopter Society 55th Annual Forum*, May 1999.

[3]Potsdam, M. and Strawn, R., "CFD Simulations of Tiltrotor Configurations in Hover," *Journal of the American Helicopter Society*, Vol. 50, No. 1, 2005, pp. 82–94.

[4]Bhagwat, M., Dimanlig, A., Saberi, H., Meadowcroft, E., Panda, B., and Strawn, R., "CFD/CSD Coupled Trim Solution for the Dual-Rotor CH-47 Helicopter Including Fuselage Modeling," *AHS International Specialists' Conference on Aeromechanics*, January 2008.

[5]Lakshminararyan, V. and Baeder, J., "High Resolution Computational Investigation of Trimmed Coaxial Rotor Aerodynamics in Hover," *AHS International Specialists Conference on Aeromechanics*, January 2008.

[6]Lee-Rausch, E. M. and Biedron, R. T., "Simulation of an Isolated Tiltrotor in Hover with an Unstructured Overset-Grid RANS Solver," *American Helicopter Society 65th Annual Forum*, May 2009.

[7]Buning, P. G., Jespersen, D. C., ad William H. Chan, T. H. P., Slotnick, J. P., Krist, S. E., and Renze, K. J., "OVERFLOW User's Manual, Version 1.8," NASA Langley Research Center, 1998.

[8]Hariharan, N. and Sankar, L., "High-Order Essentially Non-oscillatory Schemes for Rotary-Wing Wake Computations," *Journal of Aircraft*, Vol. 41, No. 2, 2004, pp. 258–267.

[9]Sankar, L., Yeshala, N., and Hariharan, N., "Application of Spatially High Order Adaptive Methods for Unsteady Flow over Rotary Wing Configurations," *International Forum on Rotorcraft Multidisciplinary Technology, American Helicopter Society Specialists Meeting, paper No. 21-1*, October 2007.

[10]Yeshala, N., Egolf, A. T., Vasilescu, R., and Sankar, L., "Application of Higher Order Spatially Accurate Schemes to Rotors in Hover," *AIAA Paper No. 2006-2818, 24th AIAA Applied Aerodynamics Conference*, June 2006.

[11]Duque, E., Sankar, L., Menon, S., Bauchau, L., Ruffin, S., Smith, M., Ahuja, K., Brentner, K., Long, L., Morris, P., and Gandhi, F., "Revolutionary Physics-based Design Tools for Quiet Helicopters," *AIAA Paper 2006-1068, 44th AIAA Aerospace Sciences Meeting*, Jan 2006.

[12]Wissink, A., Potsdam, M., Sankaran, V., Sitaraman, J., Yang, Z., and Mavriplis, D., "A Coupled Unstructured-Adaptive Cartesian CFD Approach for Hover Prediction," *AHS Society 66th Annual Forum*, May 2010.

[13]Oliver, T. and Darmofal, D., "Impact of turbulence model irregularity on high-order discretizations," AIAA-Paper 2009-0953.

[14]Burgess, N., Nastase, C., and Mavriplis, D. J., "Efficient Solution Techniques for Discontinuous Galerkin Discretizations of the Navier-Stokes Equations on Hybrid Anisotropic Meshes," AIAA Paper 2010-1448, Presented at the 48th AIAA Aerospace Sciences Meeting, Orlando FL.

[15]Sitaraman, J. and Baeder, J. D., "Evaluation of the Wake Prediction Methodologies used in CFD Based Rotor Airload Computations," *AIAA 24th Applied Aerodynamics Conference*, June 2006.

[16]Roe, P. L., "Approximate Riemann Solvers, Parametric Vectors, and Difference Schemes," *Journal of Computational Physics*, Vol. 43, No. 3, 1981, pp. 357–372.

[17]Jameson, A. and Yoon, S., "Lower-Upper Implicit Schemes with Multiple Grids for the Euler Equations," *AIAA Journal*, Vol. 25, No. 7, 1987, pp. 929–935.

[18]Sitaraman, J., Datta, A., B., D., J., and Chopra, I., "Coupled CFD/CSD Prediction of Aerodynamic and Structural Dynamic Loads for Three Critical Flight Conditions," *Presented at the 31st European Rotorcraft Forum*, Sept 2005.

[19]Mavriplis, D. J., "Results from the Third Drag Prediction Workshop Using the NSU3D Unstructured Mesh Solver," *AIAA-2007-0256, 45th AIAA Aerosciences Conference*, January 2007.

[20]Wissink, A., Sitaraman, J., Sankaran, V., Mavriplis, D., and Pulliam, T., "A Multi-Code Python-Based Infrastucture for Overset CFD with Adaptive Cartesian Grids," *AIAA-2008-0927, 46th AIAA Aerosciences Conference*, Jan 2008.

[21]Nastase, C. and Mavriplis, D. J., "High-Order Discontinuous Galerkin Methods Using a Spectral Multigrid Approach," *Journal of Computational Physics*, Vol. 213, No. 1, March 2006, pp. 330–357.

[22]Nastase, C. and Mavriplis, D. J., "A Parallel hp-Multigrid Solver for Three-Dimensional Discontinuous Galerkin Discretizations of the Euler Equations," AIAA Paper 2007-0512.

[23]Shahbazi, K., Mavriplis, D. J., and Burgess, N., "Multigrid Algorithms for high-order Discontinuous Galerkin discretizations of the compressible Navier-Stokes equations," *Journal of Computational Physics*, Vol. 228, No. 21, Nov. 2009, pp. 7917–7940.

[24]Fidkowski, K. J., Oliver, T. A., Lu, J., and Darmofal, D., "p-Multigrid solution of high-order Discontinuous Galerkin Discretizations of the Compressible Navier-Stokes equations," *Journal of Computational Physics*, Vol. 207, No. 1, 2005, pp. 92–113.

[25]Alonso, J., Hahn, S., Ham, F., Herrmann, M., Iaccarino, G., Kalitzin, G., LeGresley, P., Mattsson, K., Medic, G., Moin, P., Pitsch, H., Schlüter, J., Svärd, M., Van der Weide, E., You, D., and Wu, X., ""CHIMPS: A High-Performance Scalable Module for Multi-Physics Simulations"," *42nd AIAA/ASME/SAE/ASEE Joint Propulsion Conference*, July 2006.

[26]Sitaraman, J., Katz, A., Wissink, A., and Sankaran, V., "Evaluation of a Multi-Solver Paradigm for CFD using Unstructured and Structured Adaptive Cartesian Grids," *AIAA-2008-0660, 46th AIAA Aerosciences Conference*, Jan 2008.

[27]McAlister, K. W. and Takahashi, R. K., "NACA 0015 wing pressure and trailing vortex measurements, Research Report NASA TP 3151," Tech. rep., NASA Ames Research Center, 1991.